JOC The Journal of Organic Chemistry

Article

pubs.acs.org/joc

Computational Study of Gold-Catalyzed Homo- and Cross-Coupling Reactions

Olalla Nieto Faza* and Carlos Silva López

Departamento de Química Orgánica, Universidade de Vigo, Campus As Lagoas, 32004 Ourense, Spain

Supporting Information

ABSTRACT: The role of gold as the organizing metal in homo- and cross-coupling reactions is explored in this paper combining DFT calculations with QTAIM, NBO, and the energetic span model analysis. For the gold(III) complex **7**, a key intermediate in the experimental oxidative coupling scheme by Zhang et al., we describe the mechanisms corresponding to a cross-coupling after transmetalation with boron compounds and to a homocoupling after transmetalation with the original gold(I) complex **6**, a new example of dual role of this metal in homogeneous catalysis. We predict for the first path a two-step transmetalation with a low energy rate-limiting step characterized by a four-center transition structure, where fluorine plays an essential role, followed by a reductive elimination where the C−C bond formation is coupled to the departure of fluorine from the gold center. The homocoupling path follows a similar mechanism, with a two-step transmetalation with interesting changes in bonding around the Au(I) center and a rate-limiting reductive elimination. Our findings on the competition between mechanisms, and the effect of ligands and solvent, agree with the experimental results and provide new insights into the mechanism of gold-catalyzed cross-coupling reactions.

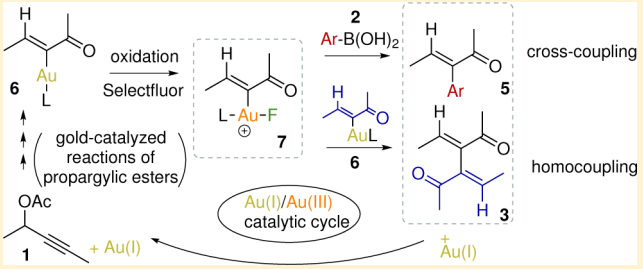

INTRODUCTION

Cross-coupling reactions are some of the most interesting processes in organic synthesis, since they allow the formation of C−C or C−heteroatom bonds in a very versatile way.

Gold can be used in these kinds of transformations through different approaches:

1. As a transmetalation agent in palladium-catalyzed cross-coupling mechanisms.[1−5]
2. As the metallic center in conventional cross-coupling reactions.[6−9] There has been fierce controversy as to whether cationic gold could catalyze these processes without the involvement of other transition metals, because of the high redox potential[10] for the AuI/AuIII pair (ε_0 = +1.41 V), which makes oxidative additions on gold centers problematic.[11] It is believed, however, that gold nanoparticles can avoid this problem, as has been shown for the Sonogashira reaction.[12,13]
3. In oxidative cross-couplings, using an external oxidant to overcome the unfavorable oxidative addition step that hinders cross-coupling cycles on gold centers. This oxidant is most commonly Selectfluor,[14] but PhI(OAc)$_2$[15] or tBuOOH[16] can also be used. Examples of this approach can be found, among others, in the recent review articles by Hopkinson et al.[17] and Wegner et al.[18]

With the aim of exploring the multifaceted role of gold in cross-coupling reactions we selected the chemistry recently developed by Zhang et al.,[14,19] who expanded the carboheterofunctionalization of alkenes with organometallic reagents (arylboronic acids) to the application of the Au(I)/Au(III) catalytic cycles made possible by the use of external oxidants[20] (Figure 1). The first part of the mechanism proposed by the authors (the steps connecting **1** with **6**) involves a set of well-known gold(I)-catalyzed reactions that we are not going to describe here.[21] The focus of this work is to describe what happens after the gold(I) complex **6**, product of these rearrangements, is oxidized to the corresponding gold(III)

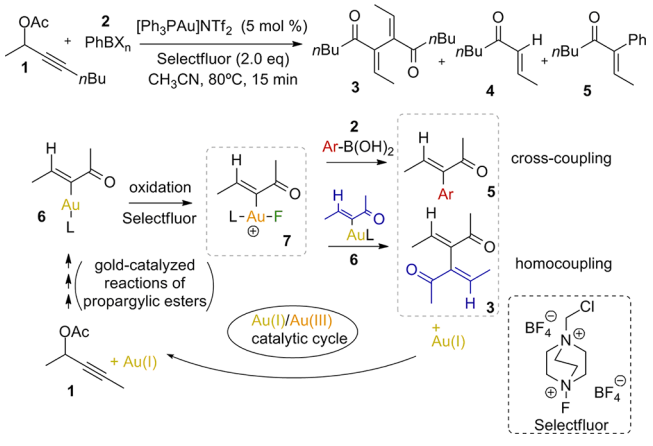

Figure 1. Main products of the reaction described by Zhang et al.[14] (top). Cross-coupling and homocoupling mechanisms starting from the oxidized Au(III) complex **7** (bottom).

Received: March 18, 2013
Published: April 18, 2013

   dx.doi.org/10.1021/jo4005603 | J. Org. Chem. 2013, 78, 4929−4939

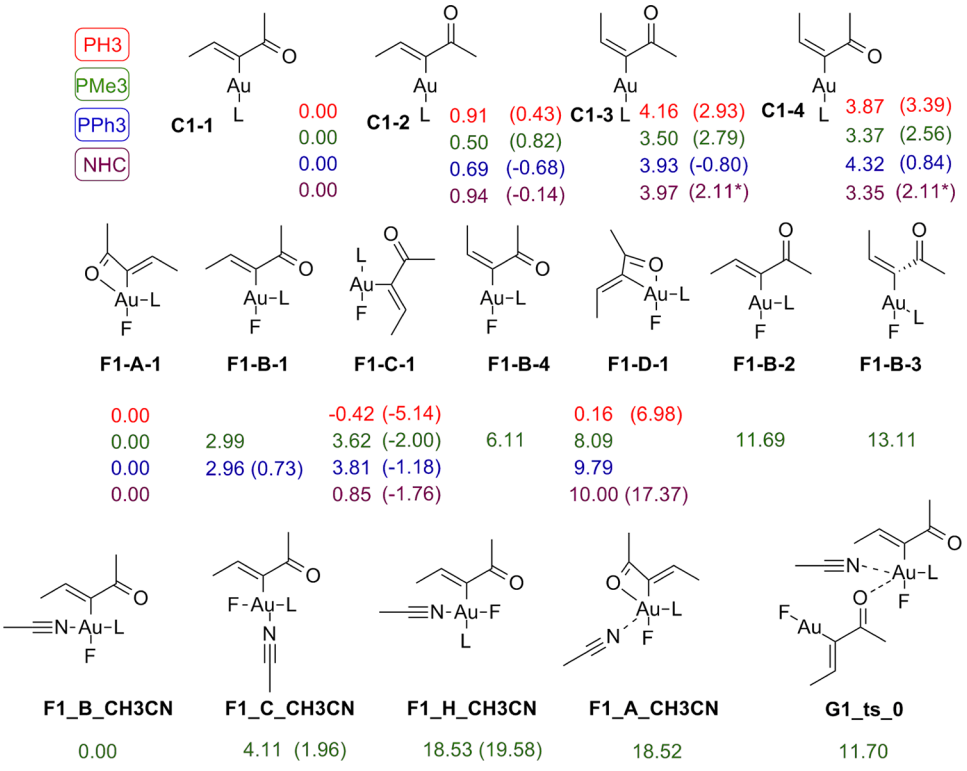

Figure 2. Different structures and conformations for the starting gold(I) (**C1** series) and gold(III) (**F1** series) complexes. The free energies (kcal/mol) in gas phase and (in acetonitrile) are expressed relative to those of **C1-1** and **F1-A-1**, respectively. The colors indicate the ligand used in each case: red, L = PH_3; green, L = PMe_3; blue, L = PPh_3; purple, L = NHC (where NHC = 1,3-dimethylimidazol-2-ylidene). In **F**, the letters A, B, etc. denote different geometries on the gold center and the descriptors 1, 2, etc. refer to the conformations of the enone moiety. In the last row, we have included tetracoordinated Au(III) complexes with a solvent molecule as the fourth ligand, together with the transition state found for the exchange of CH_3CN with **6** on gold's coordination sphere.[22]

complex **7** using Selectfluor as an external oxidant. After the formation of **7**, Zhang et al.[14] found that three products are obtained in proportions that depend on the reaction conditions. Formation of the cross-coupling product (**5**) is maximized (72% yield) with Ph_3PAuCl as a catalyst and $PhB(OH)_2$ in a 20:1 mixture of acetonitrile and water, whereas homocoupling (product **3**) is favored (60−66% yields) when $Ph_3PAuNTf_2$ and dialkoxylphenylboronates (PhB(pin) or $PhB(OCH_3)_2$) in acetonitrile are used.

We have chosen $PhB(OH)_2$ as our model boron reagent both because it maximizes the formation of the cross-coupling product in the experiments and because of the simplicity of its structure in terms of number of atoms and conformational variability, which will reduce the demand of computational resources.

The second mechanism is supposed to proceed in absence of the boronic acid or when the transmetalation of this reagent is not very efficient. In this case, the nonoxidized Au(I) complex **6** is able to transmetalate its enone moiety to a Au(III) center, on which the C−C bond formation that leads to homocoupling proceeds through a reductive elimination. Despite homocoupling products not being the most sought of in synthesis, this mechanism is of special conceptual interest since it would involve gold in a dual role both as the organizing metallic center in the coupling process (transition metal behavior) and as a transmetalation agent (metalloid behavior).

We will not study the formation of the minor product **4**, as this enone is expected to be the result of a frequently reported process of protodeauration of either **6** or **7**.

RESULTS AND DISCUSSION

Before starting with the study of the two reaction paths, our first calculations involved the exploration of different ligand arrangements and conformations of the starting gold(I) complex (which also participates further in the homocoupling mechanism) and its gold(III) oxidation product (see Figure 2).

For the gold(I) complex **C1** we find that the geometry around the metal center is always linear and that the preferred conformation of the enone moiety is in most cases **C1-1**. In this conformation, the allylic strain is minimized and a favorable electrostatic interaction can be established between the lone pair of the carbonyl oxygen and the gold center. This latter interaction seems to be less important in solution, with conformations where the oxygen is trans to gold less destabilized or even more stable than **C1-1**. Due to the large 1,3-allylic strain between the two methyl groups, **C1-4** is the less stable conformation in all cases (except for L = PMe_3)

For the gold(III) complexes, the main structural features are the geometry of the ligands around the gold center and the conformation and geometry of the enone moiety. We have found that the *s-trans*-(Z)-enone that is more stable for **C1** is also preferred here. The most stable structure in gas phase among those studied for this work (see Figure 2) is thus **F1-A-1**, where the coordination of the Au(III) center is completed with the carbonyl oxygen, whereas in solution, the open structure **F1-C-1** is more favored.

In all the complexes where gold is three cordinated, its ligands adopt a T-shaped geometry. Structures where fluorine is collinear with gold and the carbon or phosphorus ligands could

dx.doi.org/10.1021/jo4005603 | J. Org. Chem. 2013, 78, 4929−4939

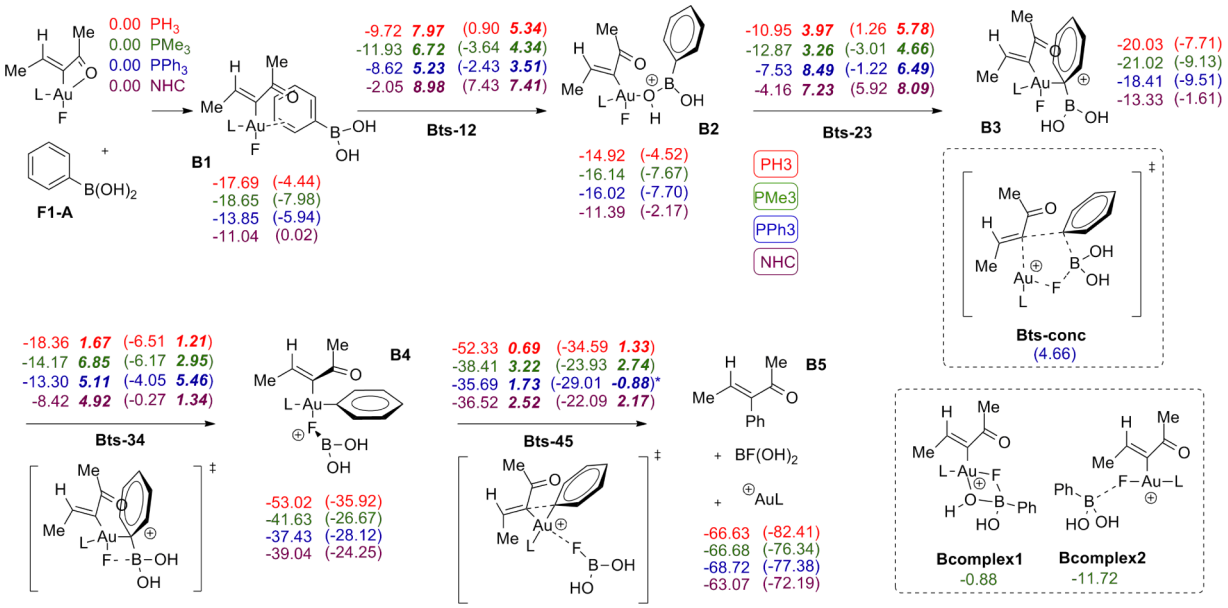

Figure 3. Mechanism proposed for the cross-coupling reaction of the carbon chain on gold(III) complex **F1** with phenylboronic acid. Free energies (kcal/mol) in gas phase and (in acetonitrile) are expressed relative to those of **F1-A** (the most stable tricoordinated gold(III) complex in the gas phase) and phenylboronic acid. For the transition structures, activation free energies are noted in bold italics. The colors indicate the ligand used in each case: red, L = PH_3; green, L = PMe_3; blue, L = PPh_3; purple, L = NHC, (where NHC = 1,3-dimethylimidazol-2-ylidene).

be characterized (the latter are more favorable), but we were not able to optimize any structure with collinear carbon and phosphine ligands. When the carbonyl oxygen is incorporated as a fourth ligand on gold (only a stable arrangement in the gas phase), the carbonyl group and fluorine, as well as the carbon center and the phosphine, prefer to be on the opposite vertices of the resultant square planar complexes. This can be considered an example of *trans influence* at work[24,25] with PR_3 and CH_3^- displaying large and F^- small effects.

For simplicity, since our main interest are the transmetalation and reductive elimination steps, we have considered that the starting point of both the homo- and cross-coupling mechanisms are tetracoordinated gold complexes (**B1** and **G1** in Figure 3 and Figure 6, respectively). Implicit in our choice of reference for energies, however, is the use of the most stable tricoordinated Au(III) complex (**F1-A-1**, just **F1-A** from now on), with a coordination vacancy, as the starting point. If, instead of **F1**, we want to use the solvent-coordinated, square planar **F1-B-CH3CN** (see Figure 2) as the entry point to these mechanisms, we have to consider a ligand-exchange step, previous to the formation of **B1** and **G1**. We have optimized the structures corresponding to this extra step for the homocoupling mechanism with L = PMe_3, finding that **F1-B-CH3CN** is 14.85 kcal/mol more stable than separated CH_3CN and **F1-A**. Restricted optimizations (in solution) with increasing values for the Au−N and Au−O distances starting from the structures of **F1-B-CH3CN** and **G1**, respectively, strongly suggest that this ligand exchange does not follow a dissociative path (dissociation of CH_3CN from **F1-B-CH3CN** to yield tricoordinated gold intermediate **F1-A**, which later incorporates **C1**), since in both cases the energy continuously increases upon dissociation of the ligand (see the Supporting Information). For the exchange between CH_3CN and **C1** on complex **F1-B-CH3CN** to yield **G1**, we have found an associative trigonal bipyramid transition structure (**G1-ts-0**) that preserves the original *trans* disposition of fluorine and the carbon fragment, with a well-accessible activation free energy of 11.70 kcal/mol. More complete studies about the relative stability of different tri- and tetracoordinated Au(III) complexes and the paths that connect them are being carried out but are out of the scope of this manuscript.

Cross-Coupling with Arylboronic Acids. Zhang et al. propose a mechanism for this transformation where the gold(III) complex suffers a transmetalation with the boronic acid, followed by C−C bond formation through reductive elimination, analogous to that of more conventional cross-coupling reactions.

A mechanism is proposed for the cross-coupling reaction of the carbon chain on gold(III) complex **F1** with phenylboronic acid. Free energies (kcal/mol) in the gas phase and (in acetonitrile) are expressed relative to those of **F1-A** (the most stable tricoordinated gold(III) complex in the gas phase) and phenylboronic acid. For the transition structures, activation free energies are noted in bold italics. The colors indicate the ligand used in each case: red, L = PH_3; green, L = PMe_3; blue, L = PPh_3; purple, L = NHC, (where NHC = 1,3-dimethylimidazol-2-ylidene).

The first step in this mechanism (see Figure 3) involves the coordination of the Au(III) center to the aryl fragment (**B1**). This process is exothermic with the three phosphine ligands and almost thermoneutral when considering the N-heterocyclic carbene.

To test alternatives to **B1** as a starting point for the mechanism, other boronic acid−gold(III) complexes were considered for L = PMe_3. Geometry optimizations starting from **F1-B** with boron directly attached to the fluorine on gold converge to **B2**. Similar attempts starting from the more stable **F1-C** converge to either unbound structures such as **Bcomplex2** (F−B distance 2.62 Å) or cyclic structures such as **Bcomplex1**, where the boronic acid bonds the fluorine through the boron atom at the same time it provides an oxygen to complete the coordination sphere of the gold(III) center. Either case results in higher free energies than those found for

dx.doi.org/10.1021/jo4005603 | J. Org. Chem. 2013, 78, 4929−4939

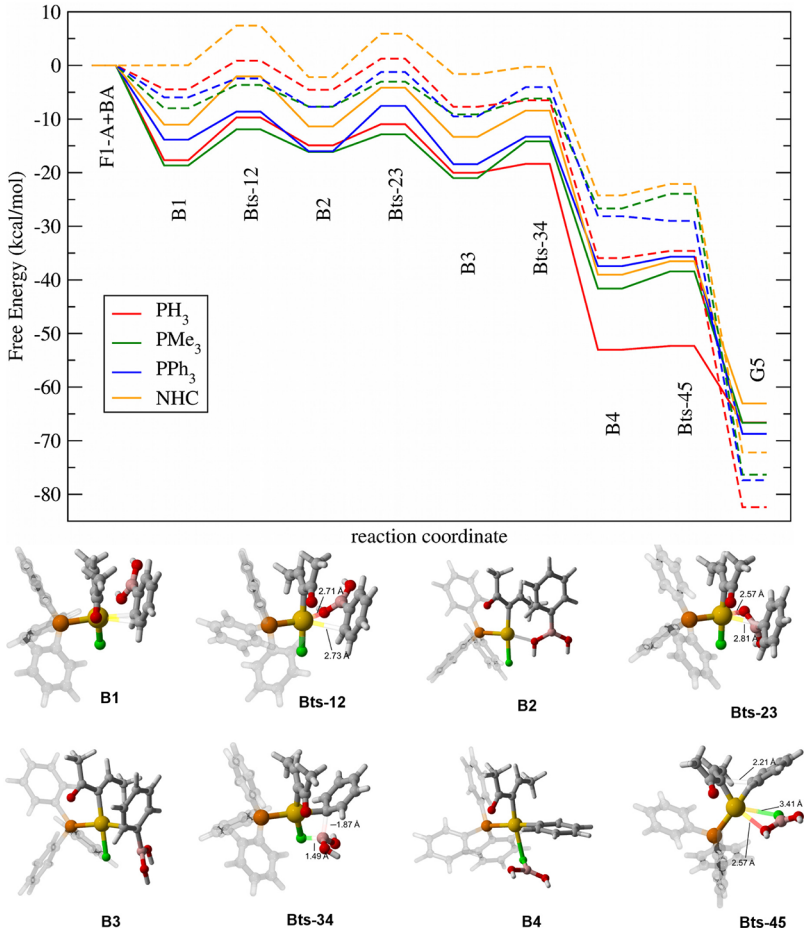

Figure 4. Reaction free energy profile in gas phase (solid lines) and in solution (dashed lines) for the mechanism in Figure 3. The different substituents used are represented with the same color code: red, L = PH_3; green, L = PMe_3; blue, L = PPh_3; yellow, L = NHC, (where NHC = 1,3-dimethylimidazol-2-ylidene). Bottom: 3D representation of the structures involved in the mechanism using PPh_3 as a ligand.

the analogous structures along the proposed mechanism (**B1**, **B2** or **B3**).

B1 is then proposed to proceed to the most stable complex we could find between **F1** and phenylboronic acid, **B3**, through two relatively low-lying transition states: **Bts-12** and **Bts-23**. Both of them involve a rocking motion of the boronic acid, which displaces its coordination site with the gold center; between the unsaturation and an oxygen in **B-ts12** and between this oxygen and the boron-attached carbon in **Bts-23**.

The stability of the three complexes (**B1**, **B2**, or **B3**) with respect to the boronic acid and **F1** used as origin of energies depends on the group used as **L** following the PPh_3 > PMe_3 > PH_3 > NHC trend, with the exception of **B1** where L = PMe_3 is more stable than L = PPh_3 (in **B2** they are almost equivalent). For the two transition structures connecting them, the stability decreases in the PMe_3 > PPh_3 > PH_3 > NHC order.

After the formation of **B3**, the transmetalation of the aryl fragment on boron is completed in a very favorable and irreversible step with a barrier of only 5.46 kcal/mol for L = PPh_3. In the corresponding transition structure a new F−B bond is formed while the B-Ph bond breaks. Although concerted, this transition state is rather asynchronous, as can be appreciated looking at its geometry (Figure 4) or the reaction path resulting from an IRC calculation (see movie in the Supporting Information).

C−C bond formation then proceeds on the resultant **B4** complex through an almost barrierless four-center transition state where the two carbon fragments on the metallic center are coupled at the same time that fluoroboronic acid is expelled from gold's coordination sphere.

Thus, transmetalation in this mechanism is a two-step process, with a first step (**Bts-23**) where the Au−C bond with the second carbon fragment (a phenyl group in this system) is formed, followed by a second step (**Bts-34**) where the C−B bond on this fragment is broken. In contrast with transmetalations in other cross-coupling reactions,[26,26] where these two events take place in concert, the complete transference of the ligand on the metal center that is exchanged for the carbon chain does not occur until the reductive elimination step (**Bts-45**).

In this context, it is interesting to discuss the role of fluorine in the transmetalation. AIM analysis of the electron density on the stationary points in this mechanism (L = PPh_3, solvent) allows the detection of a weak F−B interaction in **B3** ($\rho(BCP)$ = 0.03), which is considerably enhanced in **B4** ($\rho(BCP)$ = 0.17) and, obviously, even more in **Bts-45** ($\rho(BCP)$ = 0.19), where fluorine is removed from gold's coordination sphere. These data correlate well with the values for Wiberg's bond indices between boron and fluorine: 0.11 in **B3**, 0.66 in **B4** and 0.75 in **Bts-45**. Thus, the fluorine atom, crucial in the second part of the transmetalation (the complete exchange of the carbon fragment provided by the boronic acid in **Bts-34**), already helps stabilize complex **B3** (B−F distance 2.262 Å), where a weak Au(III)−Ph bond is first formed (with a Au−Ph distance of

dx.doi.org/10.1021/jo4005603 | J. Org. Chem. 2013, 78, 4929−4939

Table 1. Relative Free Energies (kcal/mol) for the Stationary Points Involved in the Cross-Coupling Mechanism with Different Halogens on the Au(III) Center[a]

X	OH	F	Cl	Br	I
B1	0.00	0.00	0.00	0.00	0.00
Bts-12	6.50 (6.50)	4.34 (4.34)	6.18 (6.18)	6.76 (6.76)	5.73 (5.73)
B2	0.73	0.31	−0.01	0.30	−0.43
Bts-23	4.58 (3.85)	4.97 (4.66)	4.00 (4.01)	6.75 (6.45)	5.78 (6.21)
B3	−6.92	−1.15	1.14	2.70	2.33
Bts-34	−6.15 (0.77)	1.81 (2.95)	25.19 (24.05)	28.98 (26.29)	31.02 (28.69)
B4	−34.24	−18.69	8.67	14.93	17.34
Bts-45	−26.80 (7.44)	−15.96 (2.74)	13.15 (4.48)	20.58 (5.65)	23.08 (5.75)

[a]**B1** is taken as the origin of energies for all systems. The activation energies for transition states are given between parentheses.

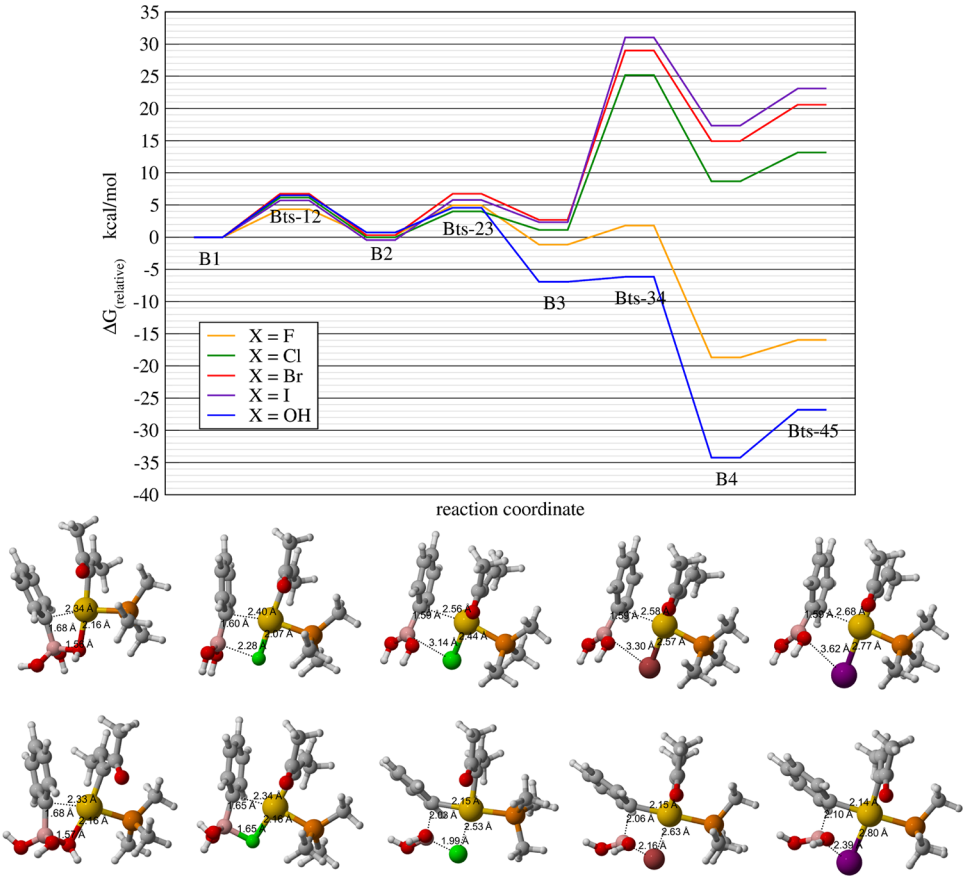

Figure 5. Reaction free energy profile for the cross-coupling mechanism (Figure 3) in solution in which fluorine has been replaced by other groups (X = OH, F, Cl, Br, I) and L = PPh_3. The energies are in kcal/mol. In the lower part of the figure, the structures of **B3** (first row) and **Bts-34** (second row) are depicted, together with the interatomic distances most relevant to the mechanism. The ordering is, from left to right, X = OH, F, Cl, Br, I in both.

2.428 Å and $\rho(BCP)$ = 0.05, compared with a Au−C distance of 2.04 Å and $\rho(BCP)$ = 0.14).

It is worth noticing that the B−C bond has already disappeared in **Bts-34** and that no bond critical point (BCP) is found between C and Ph in **B4**, although the Wiberg bond index for this pair of atoms is non negligible at a value of 0.22 (it increases to 0.46 in **Bts-45**, as expected). Also, in **B4**, the fluorine−boron bond is completely formed (B−F distance 1.366 Å), and the Au−Ph bond has also been consolidated, with $\rho(BCP)$ = 0.13 and a Au−Ph distance of 2.057 Å, which makes the transmetalation complete.

Another interesting feature are the values of NBO bond indices for the bonds in which gold is involved. They consistently display low values (∼0.6) that are later complemented by strong secondary orbital interactions. These results agree with the relatively low values for the electron density at the corresponding bond critical points: ∼0.14 for Au−C bonds, ∼0.09 for Au−F bonds and ∼0.10 for Au−P bonds, which get reduced to 0.13, 0.03 and 0.08, respectively, in **B4**, with a formally tetracoordinated gold(III) center (compare with values around 0.3 for C−C or C−H bonds, or 0.4 for carbonyl bonds).

As is the case for the gold complexes in Figure 2, $H(BCP)$ < 0 for all bonds to gold, allowing their classification as covalent interactions with partial ionic character (specially large for the Au−F bond). As expected from the accepted bonding models for this kind of gold complexes, the values of H(**r**) and ρ(**r**) indicate that the Au−L bond is remarkably more covalent when

dx.doi.org/10.1021/jo4005603 | J. Org. Chem. 2013, 78, 4929−4939

L = NHC than the Au−P interaction found with the phosphine ligands.

A very similar intramolecular aminoarylation reaction of alkenes and arylboronic acids catalyzed by the Au(III) obtained by oxidation of Au(I) with Selectfluor was also independently described by Toste et al.[27,28] and by Zhang et al.[20] In line with the findings of Toste et al. for the gold-catalyzed oxidative hereroarylation of alkenes,[28] we tried to characterize a five-center bimolecular reductive elimination transition structure that would bypass the transmetalation steps in this cross-coupling mechanism. Such a transition structure was optimized for L = PPh_3 (see **Bts-conc** in the insert in Figure 3), with a relative energy of 4.66 kcal/mol, about 6 kcal/mol more unstable than **Bts-23**, the highest energy stationary point along the proposed path. The main difference between the two systems is their use of a tetracoordinated Au(III) complex (and a different carbon chain as coupling fragment), which would make unfeasible a stepwise transmetalation such as that proposed in our work, since it would involve a pentacoordinated gold center in **B3**/**B4**. However, the free energy profile inferred from the relative energies in Figure 3, with the low barriers predicted for **Bts-34** and **Bts-45**, makes a collapse of some of these stationary points feasible upon changes in the electronic properties of the fragments involved in the reaction, connecting our stepwise process with the concerted mechanism of Toste et al.

The rate-limiting step of this mechanism is the formation of the bond between the gold center and the ipso carbon on **Bts-23**, both because of the high energy associated to this transition structure and the increase in stability that is achieved in **B3** and, specially in **B4** after a low barrier transition state. The whole mechanism is characterized by low energy barriers (the highest being 6.49 kcal/mol) that make the cross-coupling product the major experimental product under the studied reaction conditions.

The energetic span model[29] has been applied to this system using AUTOF[30] to confirm these results. For all ligands, the turnover frequency determining transition state (TDTS) is **Bts-23**, while the turnover frequency determining intermediate (TDI) can be either **B2** (for L = PPh_3, NHC) or **B1** (for L = PH_3, PMe_3). Thus, since in the latter case the energies of **B1** and **B2** are very close, the calculated energetic span (δE) for the four studied mechanisms almost coincides with the activation barrier corresponding to the **B2**−**B3** step (with values of 5.70, 4.97, 6.48, and 8.09 kcal/mol for L = PH_3, PMe_3, PPh_3 and NHC, respectively). In this case, the use of one ligand or another in the calculations does not fundamentally alter the key features of the mechanism: geometry of the intermediates and transition structures, determining steps or even rough energy profile, but definitely affects the energetic span, with values within a window of about 3 kcal/mol.

Since the fluorine atom seems to play a key role in the transmetalation process, we decided to test the extent of its relevance by replacing fluorine by other halogens and OH (X = OH, F, Cl, Br, I) and calculate the resulting reaction profiles for the cross-coupling mechanism. For simplicity, we have directly used geometry optimizations in solution with L = PMe_3.

From the results in Table 1 and Figure 5 we appreciate that up until **Bts-23** the five profiles are well matched, spreading a bit in relative energy for **B3**. The trend of the stability of this complex with X is the trend that will prevail in all structures further along the cross-coupling mechanism: OH > F > Cl > Br > I. After **B3**, the barrier corresponding to the transmetalation is almost nonexistent for X = OH, very low for X = F, and rather large for the other three halogens (increasing in the direction Cl < Br < I).

When using NBO bond indices to characterize bonding[31] (see the Supporting Information for a table with all the relevant values), we find that the main feature setting apart **B3-OH** and **B3-F** from the equivalent structures with the heavier halogens is the extent to which the B−X bond is formed, and the resultant stabilization of the complex: the interaction is strong when X = OH (0.51 bond index), considerably weaker, but well-defined, when X = F (0.11 bond index) and virtually nonexisting for the other structures (values for the bond index ranging between 0.02 and 0.04). This interaction, which highlights the key role of fluorine in the cross-coupling mechanism, also leads to low energy, early **ts-34** transition states for X = F and X = OH (in the latter case, the structure barely changes from that of **B3**). In **ts-34**, the Ph fragment is being transferred from boron to gold, which is reflected in a weakened B−Ph bond and a forming Au−Ph bond. These changes in bonding are much more pronounced for the heavier halogens (bond indices going from 0.77−0.78 in **B3** to 0.30−0.35 in **ts-34** for B−Ph and from 0.10−0.12 to 0.37−0.40 for Au−Ph) than for F (B−Ph bond index going from 0.75 to 0.70 and Au−Ph bond index going from 0.16 to 0.18). At the same time these changes are taking place, the B−X bond becomes stronger, but the extent of this strengthening is much higher for X = Cl, Br, I (B−X bond indices between 0.67 and 0.71) than for X = F, OH (B−X bond index of 0.38 for X = F), especially if we take into account that this interaction was already present in **B3** for the latter ligands. Thus, the geometry constraints imposed by the increasingly longer Au−X bonds when going from X = F to Cl, Br, and I, make the four-center **ts-34** transition state, considerably later, more asynchronous and higher in energy.

Fluorine also provides the lowest barrier for the reductive elimination step, at 2.74 kcal/mol, but the other barriers range from 4.5−7.4, making them affordable if not for the high barrier of the previous step and the resultant destabilization of **B4**.

Thus, the involvement of fluorine as a gold ligand in this mechanism seems to be not simply a side result of the use of Selectfluor as an oxidizing agent but a required element for a favorable cross-coupling mechanism, especially important in providing a low energy path for the transmetalation.

Homocoupling. The second path studied, leading to the homocoupling product, is less useful than the cross-coupling in terms of synthetic applications but provides interesting insights into gold catalysis with an example in the same mechanism of its dual behavior as either a classic transition metal or as a transmetalation agent.

Taking **F1-A** and **C1** as reference for the calculation of free energies, we start this mechanism from complex **G1** where the gold(III) center adopts a square planar geometry, completing its coordination with the oxygen on the carbonyl group of the gold(I) complex. The gold(I) center in **G1** is linear, as is most common with Au(I) complexes.

Alternative entry points to the cycle, other than complex **G1**, have also been studied, but we have relegated them to the Supporting Information. Although some structures which place the two gold atoms at an interacting distance and complete the coordination of the Au(III) center with the carbonyl oxygen of the Au(I) ligand are lower in energy than **G1** and **G2**, the transition states that lead from them to structures analogous to **G3** are either considerably more energetic than the alternatives

dx.doi.org/10.1021/jo4005603 | J. Org. Chem. 2013, 78, 4929−4939

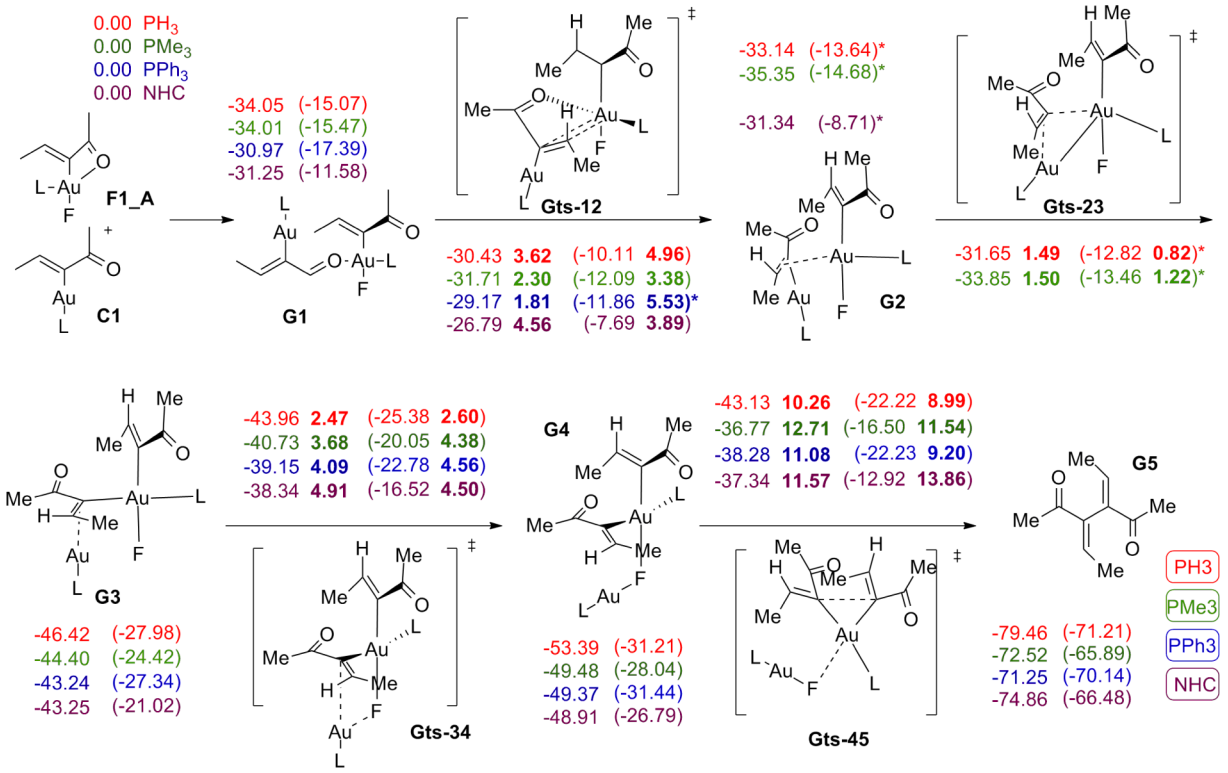

Figure 6. Mechanism proposed for the homocoupling reaction of the carbon chain on gold(III) complex **F1** a nonoxided gold(I) moiety **C1**. Free energies (kcal/mol) in gas phase and (in acetonitrile) are expressed relative to those of the starting complex **G1** For the transition structures, activation free energies are noted in bold italics. The colors indicate the ligand used in each case: red, L = PH_3; green, L = PMe_3; blue, L = PPh_3; purple, L = NHC, (where NHC = 1,3-dimethylimidazol- 2-ylidene). Where an asterisk is placed besides a parentheses, it means that these solvent data correspond to single point energy calculations in solution on the gas-phase optimized geometries (using gas-phase frequencies to calculate thermal properties).[32]

in the mechanism in Figure 6 or lead to a trans disposition of the two carbon chains on the Au(III) center in **G3** that is unsuitable for the required reductive elimination (see the Supporting Information for further information).

Thus, after the formation of **G1**, a low energy transition state exchanges the positions of the oxygen and the Au(I)-bonded olefin at the Au(III) center, resulting in an intermediate **G2** where the same enone is bonded to two gold atoms: to Au(I) through a σ bond and to Au(III) through a π interaction.

Next, we found a very interesting process for the transmetalation, occurring either through a very low barrier TS or through a barrierless downhill path. It involves a first step where the coordination of the enone that comes from the **C1** fragment switches from σ-bonding to Au(I) and η^2-bonding to Au(III) in **G2** and to η^2-bonding to Au(I) and σ-bonding to the Au(III) center in **G3**. After this, the transmetalation is completed through **Gts-34**, a transition structure with many similarities to **Bts-34**. In this step, again characterized by a low barrier, the Au(I) center detaches itself from its carbon ligand to form a new bond with the fluorine atom still coordinated to Au(III). **G4** then undergoes a four-center reductive elimination, where the two carbon fragments are coupled at the same time that the Au−F bond is broken and the two gold complexes (now both as Au(I)) are separated. The activation energy for this step (varying between 9 and 14 kcal/mol) is higher than the barriers for reductive elimination on **G4**, which could be attributed to the different properties of the coupling fragments (enone−enone vs phenyl−enone). In this homocoupling mechanism, the reductive elimination is rate limiting, compared with the transmetalation in the cross-coupling path. Application of the energetic span model identifies **Gts-45** as the TDTS and **G4** as the TDI for all ligands. The energetic span (δE) of the reaction is larger than that found for the cross-coupling mechanism, with values of 8.99, 11.54, 9.21, and 13.87 kcal/mol for L = PH_3, PMe_3, PPh_3, and NHC, respectively, almost identical to the corresponding activation barriers for **Gts-45**.

As with the other mechanism, we have performed NBO analysis of the wavefunctions and AIM analysis of the electron density on the stationary points along the potential energy surface.[34] The bonding patterns that arise from such analysis are clearly reminiscent of those found in the cross-coupling mechanism. Bonds to the Au(III) center display low Wiberg bond indices (Au−P [0.45−0.64], Au−F [0.26−0.38], Au−C [0.60−0.66]) that get supplemented by strong secondary orbital interactions, which draw a picture that is compatible with the values found for $\rho(BCP)$ (0.14 for Au(III)−C bonds, [0.07−0.10] for Au−F bonds and [0.09−0.11] for Au−P bonds) and $H(r)$ (all negative) for these bonds.

The specifics, however, change a little. The Au(III)−C_1 bond is not greatly altered along the reaction path (up until the reductive elimination step in **Gts-45**, for obvious reasons), with consistent $\rho(BCP)$ values of 0.14, distances between 2.03 and 2.05 Å, and Wiberg bond indices between 0.60 and 0.66. Au(III)−F and Au(III)−P bonds, however, are somewhat more variable, responding to the changes in coordination of the Au(III) center. The Au(III)−F bond is elongated (from 2.04 to 2.17 Å, with $\rho(BCP)$ ranging between 0.10 and 0.07 and Wiberg bond indices from 0.38 to 0.26) when going from **G1**

dx.doi.org/10.1021/jo4005603 | J. Org. Chem. 2013, 78, 4929−4939

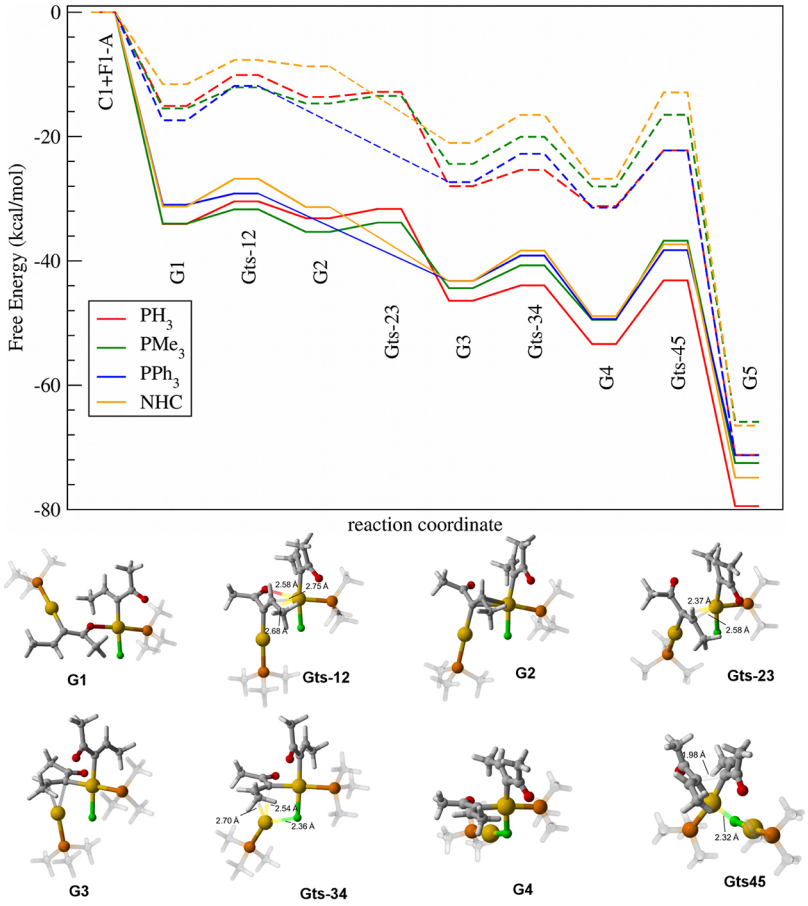

Figure 7. Reaction free energy profile in gas phase (solid lines) and in solution (dashed lines) for the mechanism in Figure 6. The different substituents used are represented with the same color code: red, L = PH_3; green, L = PMe_3; blue, L = PPh_3; yellow, L = NHC, (where NHC = 1,3-dimethylimidazol-2-ylidene). Bottom: a 3D representation of the structures involved in the mechanism is included, using PMe3 as ligand (since some of the intermediate structures could not be optimized with L = PPh_3).[33]

to **G4** a tendency also paralleled by the Au(III)−P bond (from 2.31 to 2.45 Å, with $\rho(BCP)$ ranging between 0.11 and 0.09). It is worth noting that there is a bonding interaction between Au(III) and C_2 as soon as **G2**, although the distance is still large (2.427 Å) and the $\rho(BCP)$ and Wiberg bond index small (0.06 and 0.22, respectively). This interaction increases noticeably in **G3**, with a Au(III)−C_2 distance of 2.120 Å, $\rho(BCP)$ of 0.12 and bond index of 0.45. This interaction is further enhanced in **G4**, after transmetalation has been completed, with a Au(III)−C_2 distance of 2.089 Å, $\rho(BCP)$ of 0.13, and a bond index of 0.51. This strengthening of the Au(III)−C_2 bond correlates with the weakening of the Au(I)−C_2 bond, with distances of 2.111 and 2.278 Å, values of $\rho(BCP)$ 0.15, 0.08 and bond indices 0.44 and 0.23, for **G2** and **G3**, respectively. In **G4**, the Au(I)−C_2 interaction has vanished and no BCP is found (the distance is 3.863 Å). In analogy with the cross-coupling mechanism, the fluorine atom also helps stabilize structures **G2** and **G3**, well before a full Au(I)−F bond has been established after transmetalation in **G4**. In **G2**, the Au(I)−F distance is still large, at 2.842 Å, and both the $\rho(BCP)$ and bond index are small with values of 0.019 and 0.07, respectively. The two atoms slightly approximate in **G2**, to a distance of 2.763 Å, with an accompanying increase in $\rho(BCP)$ (to 0.023) and Wiberg's bond index (0.08). In **G4** these values change to 2.112 Å, 0.08 and 0.27, respectively.

Of late, there have been reports of interactions between two (or more) gold centers enhancing catalysis[29,38] and exciting advances in the study of aurophilic interactions.[36,37] The calculations by Mendizabal and Pyykkö[38] support the existence of Au(I)−Au(III) aurophilic interactions (for the Au(I)−Au(III) distance in the dinuclear complex $Au_2(PhP(C_6H_4\text{-}S\text{-}2)_2)_2$), found experimentally to be 2.978 Å (the authors calculated with MP2 a 3.188 Å distance in a much simplified model). Other works, find Au(I)−Au(I) interactions at larger distances, such as 3.3 Å.[39] The gold−gold distances in the dinuclear complexes in the minima of the homocoupling mechanism (ranging between 3.4 and 3.6 Å) are larger than the 3.32 Å resulting from the sum of two gold's van der Waals radii, but the shorter Au(I)−Au(III) distances found in **Gts-45** (3.24 Å) prompted us to explore the possibility of metallophilic interactions between the two gold centers along the reaction path. However, AIM analysis of the electron densities for all stationary points showed no gold−gold bond critical points, and the values of bond indices obtained after an NBO analysis are very low (between 0.06 and 0.09, with an outlier at 0.13 for **Gts-45**). However, aurophilic interactions are not completely discarded and a more detailed study on the effect of ligands on the geometries and bonding patterns of these complexes are being carried out.

■ COMPUTATIONAL METHODS

We have used density functional theory in the Kohn−Sham formulation as implemented in Gaussian09[40] to locate minima and transition structures on the potential energy surfaces of the systems

dx.doi.org/10.1021/jo4005603 | J. Org. Chem. 2013, 78, 4929−4939

studied. Considering the results of our benchmark of density functionals for the structures in the "gold carousel",[41] against CCSD/def2-TZVPP//CCSD/def2-SVP data,[42] we have chosen the M06 functional[43] with the double-ζ quality def2-SVP basis set.[44] Relativistic effects, which determine a large part of gold chemistry, have been introduced through the electron core potential (ecp-60-mwb) usually associated with this basis set.[45] As in our previous work,[42] an integration grid containing 99 radial shells and 590 angular points per shell has been employed throughout the entire study.

For all stationary points, the stability of the wave function has been computed[46] and harmonic analysis of the second derivatives of the energy with respect to the nuclear displacements performed to characterize them as minima or transition structures.

Approximate reaction profiles have thus been calculated for the paths leading from **7** to **5** and **3** (see Figure 1) both in the gas phase and in acetonitrile (the most common solvent used in the experimental paper by Zhang et al.[14]). In order to simulate solvation, the polarizable continuum model (PCM) with the integral equation formalism variant (IEFPCM)[47,48] was used with UFF radii in Gaussian09 for the latter calculations (dielectric constant 35.688).

For selected structures (as indicated in the text), atoms in molecules (AIM) theory[49] and natural bond orbital (NBO) theory[50] have been used to analyze, respectively, the topology of the electron density and the wave function of the optimized structures in solution, in order to describe bonding interactions in the organometallic complexes. For the first, we have used wave functions calculated with Gaussian09 (where additional core electron density functions have been added to avoid the spurious critical points due to the use of an electron core potential for gold) with the AIMAll code;[51] for the second, the NBO3.1 code as implemented in Gaussian09.[52] The energy density $H(r)$ at the bond critical point is used to check the covalent character of bonding. As proposed by Kraka et al.,[53−55] a negative value of $H(BCP)$ denotes a covalent interaction.

Unless otherwise specified, all thermodynamic and structural parameters mentioned in the text refer to the reaction paths optimized in solution.

For the visualization of results and preparation of figures in the paper, Molden[56] and Cylview[57] have been used. The AUTOF program in its Excel version[30] has been used to calculate the energetic span (δE) and turnover frequency determining transition states (TDTS) and intermediates (TDI) in the context of Kozuch's energetic span model.[29]

In order to reduce the computational cost, the *n*-butyl side chain used in the experimental paper has been replaced by a methyl group in all our calculations. In a first stage of our work, we also substituted the bulky triphenylphosphine (PPh_3) ligand on gold with trimethylphosphine (PMe_3), but later we decided to use this study as a testing ground for the soundness of such ligand simplifications, commonly used in this kind of computational mechanistic studies, comparing the reaction profiles with L = PH_3, PMe_3 and PPh_3.[58] Since N-heterocyclic carbenes are becoming more popular in gold-catalysis, due to their interesting properties[59] we have also calculated the profiles using a small NHC (1,3-dimethylimidazol-2-ylidene) in order to establish potential differences between the use of carbenes and phosphines as ligands in these mechanisms. When no other specification is added in the discussion, all the data in the text are supposed to refer to geometries optimized in acetonitrile with triphenylphosphine as a ligand. With the same goal of reducing the computational cost, we have neglected to include the counterion of the gold complex $[Ph_3PAu]^+$, which is not expected to directly affect the reaction center in this solvent

Conclusions. This work, which uses state-of-the-art computational tools to study gold-catalyzed cross-coupling reactions, provides relevant results in two areas. (1) It describes in detail the two paths available to gold(III) complex **7**, leading to new, basic information on the mechanisms involved in gold catalysis and cross-coupling processes. (2) It offers insight into the computational treatment needed for these systems.

From the mechanistic study itself, we conclude that the cross-coupling mechanism that opens when $PhB(OH)_2$ is used is the most favorable under the conditions studied, in agreement with the experimental findings (see Figure 8). It proceeds through a two-step

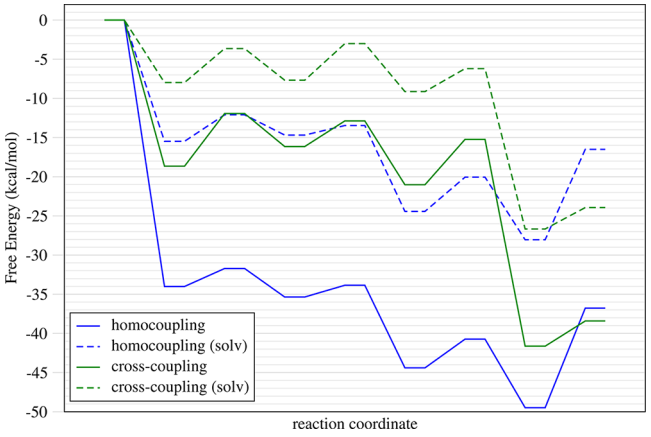

Figure 8. Comparison of the free energy profiles in gas phase (solid lines) and in solution (dashed lines) for the homo- and cross-coupling mechanisms with L = PMe_3. The cross-coupling mechanism is preferred over the homocoupling.

transmetalation, assisted by a F−B interaction, in which the B−C bond is broken (**Bts-34**) after the Au−Ph has been formed (**Bts-23**). The transference of the fluorine atom that is exchanged for the carbon chain on gold's coordination sphere upon transmetalation is only completed in the four-center reductive elimination step (**Bts-45**). The substitution of fluorine for other halogens in this mechanism, significantly alters the reaction profile, with considerably higher barriers for the transmetalation step, arising from the larger Au−X distances disturbing the four-centered transition structure. Replacement of fluorine by OH, however, leads to a lower-energy transmetalation, which makes worth exploring gold oxidation with oxygen electrophiles. The turnover frequency determining transition state (TDTS) in this mechanism is the first step of the transmetalation (**Bts-23**) for all ligands, and the energetic span values ranging between 5.0 and 8.1 kcal/mol correspond to a readily proceeding reaction.

In the absence of another transmetalation agent, Au(I) complex **C1** can transfer its enone moiety to the Au(III) center and generate a homocoupling product. This path, with energetic span values ranging between 9.2 and 13.9 kcal/mol, is not competitive with the cross-coupling with boronic acids, but it does not require a strong activation either. The main features of this mechanism are the evolution of the enone on **C1** from σ-bonding to Au(I) and η^2-bonding to Au(III) to η^2-bonding to Au(I) and σ-bonding to Au(III), the early apparition of a Au(I)−F interaction that parallels the B−F interaction found in the cross-coupling mechanism and the persistence of the Au(III)−F bond up until the reductive elimination step, in contrast to the more common concerted transmetalations found in other systems. In this mechanism, the four-center reductive elimination is the turnover frequency determining transition state (TDTS) for all ligands. Of special relevance is the dual character of gold along this path, acting both as organizing metallic center and as a transmetalation agent, which opens the way for the use of gold in more general cross-coupling reactions. In this line, it could be interesting to run experiments with different Au(III) and Au(I) salts, in order to evaluate the possibility of cross-couplings where this dual role of gold is further exploited.

Regarding the methods used to model the mechanisms, it is found that the inclusion of solvation is important. It smoothens out certain features of the potential energy surfaces, transforming some transition structures that are found in the gas-phase, in shoulders in the potential energy surface in solution. Just optimizing in gas-phase and using single-point calculations in solution to correct the results might not be enough to provide an accurate description of the mechanisms. Beyond that, the general shape of the profiles is not essentially altered in

dx.doi.org/10.1021/jo4005603 | J. Org. Chem. 2013, 78, 4929−4939

solution from the gas phase values although the free energy values can change significantly and the barriers are consistently higher. Comparison of competitive mechanisms can thus be quite off. Truncation of the ligand does not affect the general shape of the profile overmuch (although in the cross-coupling mechanism, the TDI changes when going from the smaller phosphines to PPh_3); however, the energy spans change in a window of about 3 kcal/mol for the phosphines, which may or may not be tolerable depending on the application sought.

■ ASSOCIATED CONTENT

Supporting Information

Restricted optimizations for the Au−N and Au−O distances in **G1** and **F1-B-CH$_3$CN**, alternative structures involved in the homocoupling mechanism, cross-coupling profile with L=P(=O)Me_3, a movie displaying the IRC of **Bts-34-pme3**, tables of geometric parameters, thermodynamic data, and NBO bond information, and Cartesian coordinates of all the structures mentioned in the text. This material is available free of charge via the Internet at http://pubs.acs.org.

■ AUTHOR INFORMATION

Corresponding Author

*E-mail: faza@uvigo.es.

Notes

The authors declare no competing financial interest.

■ ACKNOWLEDGMENTS

We thank the Centro de Supercomputación de Galicia (CESGA) for the allocation of computational resources, especially through the ICTS call (ICTS-227), and the University of Vigo for funding through the INOU-2012 program.

■ REFERENCES

(1) Hashmi, A. S. K.; Döpp, R.; Lothschütz, C.; Rudolph, M.; Riedel, D.; Rominger, F. *Adv. Synth. Catal.* **2010**, *352*, 1307−1314.

(2) Hashmi, A. S. K.; Lothschütz, C.; Döpp, R.; Rudolph, M.; Ramamurthi, T. D.; Rominger, F. *Angew. Chem., Int. Ed.* **2009**, *48*, 8243−8246.

(3) Man, W. Y.; Bock, S.; Zaitseva, N. N.; Bruce, M. I.; Low, P. J. *J. Organomet. Chem.* **2011**, *696*, 2172−2176.

(4) Peña López, M.; Ayán-Varela, M.; Sarandeses, L. A.; Pérez Sestelo, J. *Chem.—Eur. J.* **2010**, *16*, 9905−9909.

(5) Chan, J. M. W.; Amarante, G. W.; Toste, F. D. *Tetrahedron* **2011**, *67*, 4306−4312.

(6) González-Arellano, C.; Abad, A.; Corma, A.; García, H.; Iglesias, M.; Sánchez, F. *Angew. Chem., Int. Ed.* **2007**, *46*, 1536−1538.

(7) Kanuru, V. K.; Kyriakou, G.; Beaumont, S. K.; Papageorgiou, A. C.; Watson, D. J.; Lambert, R. M. *J. Am. Chem. Soc.* **2010**, *132*, 8081−8086.

(8) Kyriakou, G.; Beaumont, S. K.; Humphrey, S. M.; Antonetti, C.; Lambert, R. M. *ChemCatChem* **2010**, *2*, 1444−1449.

(9) Beaumont, S. K.; Kyriakou, G.; Lambert, R. M. *J. Am. Chem. Soc.* **2010**, *132*, 12246−12248.

(10) Bratsch, S. G. *J. Phys. Chem. Ref. Data* **1989**, *18*, 1−21.

(11) Lauterbach, T.; Livendahl, M.; Rosellón, A.; Espinet, P.; Echavarren, A. M. *Org. Lett.* **2010**, *12*, 3006−3009.

(12) Corma, A.; Juárez, R.; Boronat, M.; Sánchez, F.; Iglesias, M.; García, H. *Chem. Commun.* **2011**, *47*, 1446−1448.

(13) Boronat, M.; Combita, D.; Concepción, P.; Corma, A.; García, H.; Juárez, R.; Laursen, S.; López-Castro, J. d. D. *J. Phys. Chem. B* **2012**, *116*, 24855−24867.

(14) Zhang, G.; Peng, Y.; Cui, L.; Zhang, L. *Angew. Chem., Int. Ed.* **2009**, *48*, 3112−3115.

(15) Kar, A.; Mangu, N.; Kaiser, H. M.; Beller, M.; Tse, M. K. *Chem. Commun.* **2008**, 386−388.

(16) Wegner, H. A.; Ahles, S.; Neuburger, M. *Chem.—Eur. J.* **2008**, *14*, 11310−11313.

(17) Hopkinson, M. N.; Gee, A. G.; Gouverneur, V. *Chem.—Eur. J.* **2011**, *17*, 8248−8262.

(18) Wegner, H. A.; Auzias, M. *Angew. Chem., Int. Ed.* **2011**, *50*, 8236−8247.

(19) Cui, L.; Zhang, G.; Zhang, L. *Bioorg. Med. Chem. Lett.* **2009**, *19*, 3884−3887.

(20) Zhang, G.; Cui, L.; Wang, Y.; Zhang, L. *J. Am. Chem. Soc.* **2010**, *132*, 1474−1475.

(21) The interested reader can check out the studies in the litterature[41,60] where the steps involved in the gold(I)-catalyzed 1,3-migration of a propargyl ester and the evolution of the resultant allene intermediates are thoroughly discussed.

(22) When L = NHC, **C1-3** and **C1-4** in solution converge to the same structure, halfway between *s-cis* and *s-trans*.

(23) Appleton, T. G.; Clark, H. C.; Manzer, L. E. *Coord. Chem. Rev.* **1973**, *10*, 335−422.

(24) Jones, P. G.; Williams, A. F. *J. Chem. Soc., Dalton Trans.* **1977**, *15*, 1430−1434.

(25) Álvarez, R.; Pérez, M.; Nieto Faza, O.; de Lera, A. R. *Organometallics* **2008**, *27*, 3378−3389.

(26) Braga, A. A. C.; Morgon, N. H.; Ujaque, G.; Lledós, A.; Maseras, F. J. *Organomet. Chem.* **2006**, *691*, 4459−4466.

(27) Brenzovich, W. E.; Benitez, D.; Lackner, A. D.; Shunatona, H. P.; Tkatchouk, E.; Goddard, W. A., III; Toste, F. D. *Angew. Chem., Int. Ed.* **2010**, *49*, 5519−5522.

(28) Tkatchouk, E.; Mankad, N. P.; Benitez, D.; Goddard, W. A., III; Toste, F. D. *J. Am. Chem. Soc.* **2011**, *133*, 14293−14300.

(29) Kozuch, S.; Shaik, S. *Acc. Chem. Res.* **2011**, *44*, 101−110.

(30) Kozuch, S. *WIREs Comput. Mol. Sci.* **2012**, *2*, 795−815.

(31) In the discusion, we qualitatively use variations in bond indices along the reaction path, instead of directly comparing the bond indices of X = OH, F, Cl, Br, I, since some of the variations between structures with different halogens just reflect the expected variations in the percentages of ionic and covalent contributions to bonding.

(32) Transition structure **Gts-12** could be fully optimized for every ligand in gas and solution phase, except for L = PPh_3 in solution phase. A similar problem arises with the structures of **G2** and **Gts-23**, which we were only able to optimize in gas phase, and not with L = PPh3. In these cases, we have added to the data in Figure 6 an estimation of their free energies in solution using single-point solvation calculations on the gas-phase optimized geometries and the thermal corrections derived from the gas-phase frequencies.

(33) We draw a direct path between **Gts-12** and **G3**, reflecting **G2** and **Gts-23** losing their identity as stationary points while being transformed into shoulders in the potential energy surface upon solvation. This is supported by the very low values found for the barriers associated to **Gts-23** when L = PH_3 or PMe_3 (around 1.5 kcal/mol in gas phase and an estimated 1 kcal/mol in solution).

(34) In order to be able to include structures **G2** and **Gts-23** in the discussion, we have chosen the gas-phase path corresponding to L = PMe_3 for these analysis.

(35) Rodríguez, L. I.; Roth, T.; Fillol, J. L.; Wadepohl, H.; Gade, L. H. *Chem.—Eur. J.* **2012**, *18*, 3721−3728.

(36) Schmidbaur, H.; Schier, A. *Chem. Soc. Rev.* **2008**, *37*, 1931−1951.

(37) Schmidbaur, H.; Schier, A. *Chem. Soc. Rev.* **2012**, *41*, 370−412.

(38) Mendizabal, F.; Pyykkö, P. *Phys. Chem. Chem. Phys.* **2004**, *6*, 900−905.

(39) Colacio, E.; Lloret, F.; Kivekäs, R.; Suárez-Varela, J.; Sundberg, M. R.; Uggla, R. *Inorg. Chem.* **2003**, *42*, 560−565.

(40) Frisch, M. J. et al. Gaussian 09 Revision A.1, Gaussian Inc.: Wallingford, CT, 2009.

(41) Correa, A.; Marion, N.; Fensterbank, L.; Malacria, M.; Nolan, S. P.; Cavallo, L. *Angew. Chem., Int. Ed.* **2008**, *47*, 718−721.

(42) Nieto Faza, O.; Álvarez Rodríguez, R.; Silva López, C. *Theor. Chem. Acc.* **2011**, *128*, 647−661.
(43) Zhao, Y.; Truhlar, D. G. *J. Chem. Phys.* **2006**, *125*, 194101.
(44) Schäfer, A.; Horn, H.; Ahlrichs, R. *J. Chem. Phys.* **1992**, *97*, 2571−2577.
(45) Andrae, D.; Häussermann, U.; Dolg, M.; Stoll, H.; Preuss, H. *Theor. Chim. Acta* **1990**, *77*, 123−141.
(46) Bauernschmitt, R.; Ahlrichs, R. *J. Chem. Phys.* **1996**, *104*, 9047−9052.
(47) Tomasi, J.; Persico, M. *Chem. Rev.* **1994**, *94*, 2027−2094.
(48) Tomasi, J.; Menucci, B.; Cammi, R. *Chem. Rev.* **2005**, *105*, 2999−3093.
(49) Bader, R. *Atoms in Molecules: A Quantum Theory*; Oxford University Press: Oxford, 1994.
(50) Weinhold, F.; Landis, C. R. *Chem. Educ. Res. Pract. Eur.* **2001**, *2*, 91−104.
(51) Keith, T. A. AIMAll (Version 11.12.19), TK Gristmill Software, Overland Park, KS, 2011.
(52) Glendening, E. D.; Reed, A. E.; Carpenter, J. E.; Weinhold, F. NBO Version 3.1.
(53) Kraka, E.; Cremer, D. In *Theoretical Models of Chemical Bonding. The Concept of the Chemical Bond*; Maksic, Z. B., Ed.; Springer Verlag: Heidelberg, 1990; Vol. *2*; Chapter Chemical implication of local features of the electron density distribution, p 453.
(54) Cremer, D.; Kraka, E. *Croat. Chem. Acta* **1984**, *57*, 1259−1281.
(55) Cremer, D.; Kraka, E. *Angew. Chem., Int. Ed.* **1984**, *23*, 627−628.
(56) Schaftenaar, G.; Noordik, J. H. *J. Comput.-Aided Mol. Design* **2000**, *14*, 123−124.
(57) Legault, C. Y. CYLview, 1.0b (http://www.cylview.org). Université de Sherbrooke, 2009.
(58) A reviewer suggested that under the experimental conditions of the oxidation with Selectfluor the triphenylphosphine ligand can be oxidized to $POPh_3$. We were not able to find references to this chemistry, even when dealing with electrochemical oxidation studies in analogous systems,[61−63] but we decided to also explore the possibility of L being a phosphine oxide. The results are included in the Supporting Information.
(59) Nolan, S. P. *Acc. Chem. Res.* **2011**, *44*, 91−100.
(60) Soriano, E., Marco-Contelles, J., Eds. *Computational Mechanisms of Au and Pt Catalyzed Reactions*; Topics in Current Chemistry; Springer: New York, 2011.
(61) Doménech, A.; Leyva-Pérez, A.; Al-Resayes, S. I.; Corma, A. *Electrochem. Commun.* **2012**, *19*, 145−148.
(62) Simonneau, A.; Garcia, P.; Goddard, J.-P.; Mouriès-Mansuy, V.; Malacria, M.; Fensterbank, L. *Beilstein J. Org. Chem.* **2011**, *7*, 1379−1386.
(63) Leyva-Pérez, A.; Doménech, A.; Al-Resayes, S. I.; Corma, A. *ACS Catal.* **2012**, *2*, 121−126.